



Article

Differentiation of Hepatocellular Carcinoma from Intrahepatic Cholangiocarcinoma through MRI Radiomics

Ning Liu 1,2, Yaokun Wu 1, Yunyun Tao 1, Jing Zheng 1, Xiaohua Huang 1, Lin Yang 1,* and Xiaoming Zhang 10

- Medical Imaging Key Laboratory of Sichuan Province, Interventional Medical Center, Department of Radiology, Medical Research Center, Affiliated Hospital of North Sichuan Medical College, Nanchong 637000, China; 15082765186@163.com (N.L.); yaokunwu777@163.com (Y.W.); yunyuntao@163.com (Y.T.); 15082793282@163.com (J.Z.); harold1966@126.com (X.H.); zhangxm@nsmc.edu.cn (X.Z.)
- Hospital of Chengdu Office of People's Government of Tibetan Autonomous Region (Hospital. C.T.), Chengdu 610041, China
- * Correspondence: linyangmd@163.com

Simple Summary: The noninvasive differentiation of hepatocellular carcinoma (HCC) from intrahepatic cholangiocarcinoma (ICC) remains challenging. In recent years, the number of studies on the application of radiomics in liver cancer has grown dramatically. However, there have been very few studies on the differentiation of HCC from ICC based on multisequence magnetic resonance imaging (MRI) radiomics. This study aimed to investigate the efficacy of a radiomics model based on pretherapeutic fat suppression T₂-weighted imaging (FS-T₂WI) and dynamic-contrast-enhanced MRI (DCE-MRI) features obtained from the arterial phase (AP) and portal venous phase (PVP) for noninvasively differentiating HCC from ICC.

Abstract: The purpose of this study was to investigate the efficacy of magnetic resonance imaging (MRI) radiomics in differentiating hepatocellular carcinoma (HCC) from intrahepatic cholangiocarcinoma (ICC). The clinical and MRI data of 129 pathologically confirmed HCC patients and 48 ICC patients treated at the Affiliated Hospital of North Sichuan Medical College between April 2016 and December 2021 were retrospectively analyzed. The patients were randomly divided at a ratio of 7:3 into a training group of 124 patients (90 with HCC and 34 with ICC) and a validation group of 53 patients (39 with HCC and 14 with ICC). Radiomic features were extracted from axial fat suppression T₂-weighted imaging (FS-T₂WI) and axial arterial-phase (AP) and portal-venous-phase (PVP) dynamic-contrast-enhanced MRI (DCE-MRI) sequences, and the corresponding datasets were generated. The least absolute shrinkage and selection operator (LASSO) method was used to select the best radiomic features. Logistic regression was used to establish radiomic models for each sequence (FS-T₂WI, AP and PVP models), a clinical model for optimal clinical variables (C model) and a joint radiomics model (JR model) integrating the radiomics features of all the sequences as well as a radiomics-clinical model combining optimal radiomic features and clinical risk factors (RC model). The performance of each model was evaluated using the area under the receiver operating characteristic curve (AUC). The AUCs of the FS-T₂WI, AP, PVP, JR, C and RC models for distinguishing HCC from ICC were 0.693, 0.863, 0.818, 0.914, 0.936 and 0.977 in the training group and 0.690, 0.784, 0.727, 0.802, 0.860 and 0.877 in the validation group, respectively. The results of this study suggest that MRI-based radiomics may help noninvasively differentiate HCC from ICC. The model integrating the radiomics features and clinical risk factors showed a further improvement in performance.

Keywords: radiomics; hepatocellular carcinoma; intrahepatic cholangiocarcinoma; differentiation



Citation: Liu, N.; Wu, Y.; Tao, Y.; Zheng, J.; Huang, X.; Yang, L.; Zhang, X. Differentiation of Hepatocellular Carcinoma from Intrahepatic Cholangiocarcinoma through MRI Radiomics. *Cancers* **2023**, *15*, 5373. https://doi.org/10.3390/ cancers15225373

Received: 23 August 2023 Revised: 25 October 2023 Accepted: 6 November 2023 Published: 11 November 2023



Copyright: © 2023 by the authors. Licensee MDPI, Basel, Switzerland. This article is an open access article distributed under the terms and conditions of the Creative Commons Attribution (CC BY) license (https://creativecommons.org/licenses/by/4.0/).

1. Introduction

Hepatocellular carcinoma (HCC) and intrahepatic cholangiocarcinoma (ICC) are the most common types of primary liver cancer, with the former accounting for approxi-

Cancers 2023, 15, 5373 2 of 17

mately 75–85% of cases [1–3], and their morbidity rates are increasing [4–8]. The treatment strategies for and prognosis of patients with HCC and ICC are very different [2,3,9–19]. If resection is considered feasible, resection is the treatment of choice for both entities. However, only a minority of patients are candidates for curative-intent resection. In non-resectable cases, HCC mainly responds to transcatheter arterial chemoembolization, targeted therapy and immunotherapy, while ICC benefits from classical chemotherapy, targeted therapy and immunotherapy [17,20]. Therefore, accurate pretherapeutic differentiation between HCC and ICC is essential.

At present, the noninvasive differentiation of HCC from ICC remains challenging. For example, the sensitivity and specificity of various serum tumor markers, including alpha-fetoprotein (AFP) and carbohydrate antigen 19-9 (CA19-9), are unsatisfactory [21–24]. The presentation of HCC and ICC on dynamic-contrast-enhanced computed tomography (CT) and magnetic resonance imaging (MRI) is mostly typical [25–28]. However, both HCC and ICC may occur in patients with chronic hepatitis, and imaging enhancement patterns tend to be similar in some patients with both HCC and ICC [3,29–33]. In addition, the enhancement may be unremarkable or atypical in some HCC cases (especially in cases of small, hypovascular or sclerosing HCC lesions) [34–36]. Traditional medical imaging analysis relies heavily on the physician's subjective judgment and is thus prone to misdiagnosis [37]. Liver biopsy remains the gold standard for the final diagnosis, but this invasive procedure is refused by some patients [38]. Therefore, a pretherapeutic noninvasive method for distinguishing HCC from ICC is urgently needed.

Based on existing medical imaging modalities such as CT and MRI, an emerging technique called radiomics [39] can be used to convert intrinsic pathophysiological information that is invisible to the human eye into high-dimensional quantitative image features, which can then be used to perform tumor classification via an analysis of the relationship between these features and clinical/genetic data [39–41]. Studies have shown that radiomics exhibits unique advantages in classifying the disease and predicting the prognosis of patients with liver cancer [39,42–56]. However, there have been very few studies on the differentiation of HCC from ICC based on multisequence MRI radiomics to date. In this paper, the efficacy of a radiomic model based on pretherapeutic fat suppression T_2 -weighted imaging (FS- T_2 WI) and dynamic-contrast-enhanced MRI (DCE-MRI) features in the arterial phase (AP) and portal venous phase (PVP) for noninvasively differentiating HCC from ICC was investigated.

2. Materials and Methods

2.1. Patients

The pretherapeutic MRI and clinical data of HCC and ICC patients treated at the Affiliated Hospital of North Sichuan Medical College between April 2016 and December 2021 were retrospectively analyzed. The inclusion criteria were as follows: (1) a pathological diagnosis of HCC or ICC; (2) multisequence MRI of the upper abdomen performed within 4 weeks prior to treatment; and (3) no antitumor-related treatment prior to the MRI scan. The exclusion criteria were as follows: (1) combined hepatocellular cholangiocarcinoma (cHCC-CC); (2) incomplete data or poor MR image quality; and (3) lesion diameter <2 cm or unclear lesion contours. The data of 206 patients with primary liver cancer (145 with HCC and 61 with ICC) were collected, and 177 (129 with HCC and 48 with ICC) met the inclusion and exclusion criteria and were finally enrolled in this study. The patients were randomly divided at a 7:3 ratio into a training group (n = 124, 90 with HCC and 34 with ICC) and a validation group (n = 53, 39 with HCC and 14 with ICC) (Figure 1).

The following clinical data were acquired: age; sex; cirrhosis status; hepatitis B serological test results; pseudocapsule status; hemorrhagic necrosis status; extrahepatic metastasis status; portal vein tumor thrombus status; number of tumors; ascites status; maximum tumor diameter; abnormal prothrombin; AFP level; carcinoembryonic antigen (CEA) level; and CA19-9 level. The levels of tumor markers were measured within one week before treatment.

Cancers 2023, 15, 5373 3 of 17

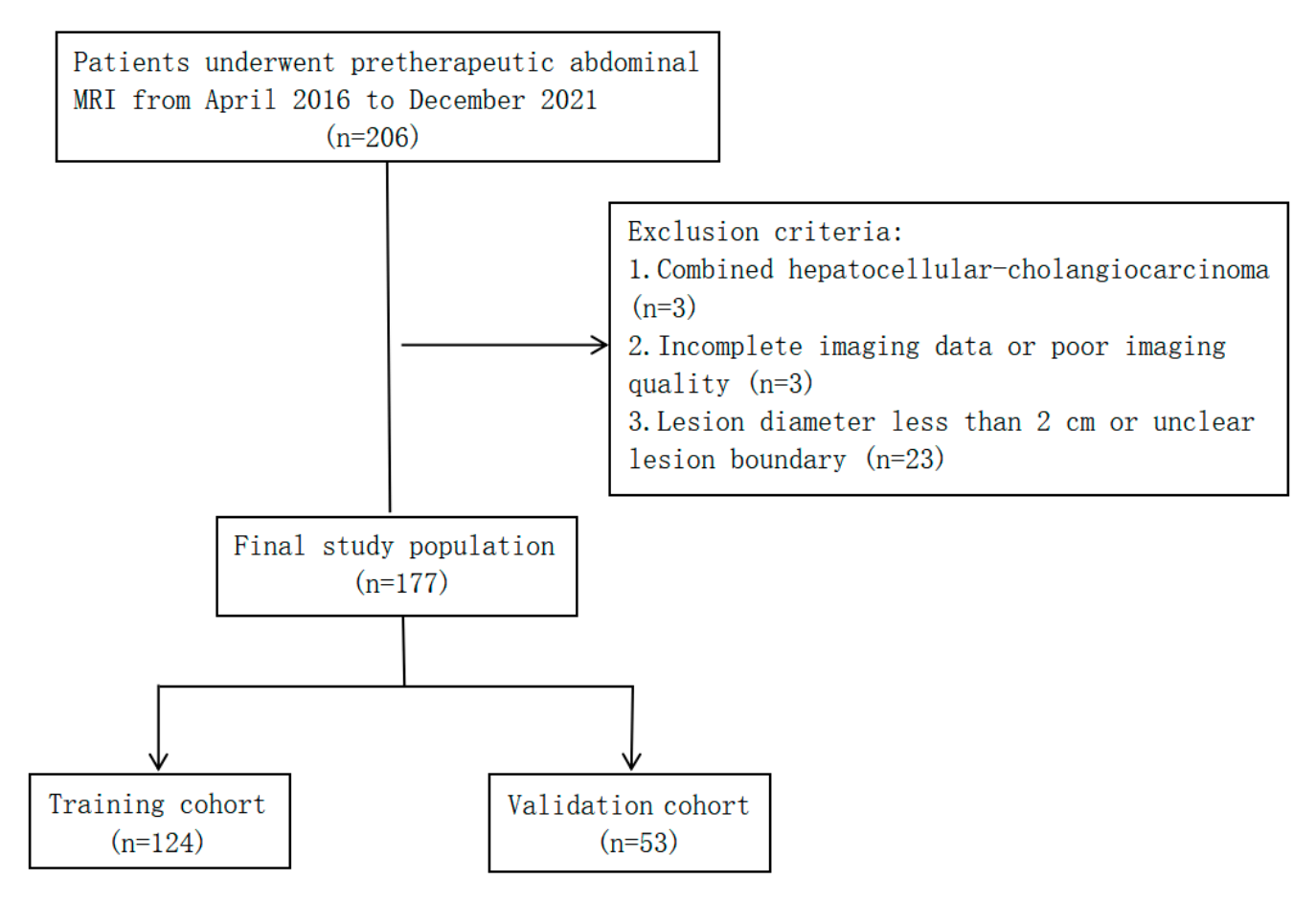


Figure 1. Flow chart of study population selection.

2.2. MRI Acquisition

MRI scans were performed using a Discovery 750 3.0 T superconductivity MRI scanner with a 32-channel phased-array surface coil (GE, USA). Prior to the MRI scans, all subjects fasted for 4 h and received training in breathing exercises. Scan sequences included axial 3D liver acceleration volume acquisition (LAVA), FS- T_2 WI and axial 3D LAVA dynamic-contrast-enhanced sequences (Table 1). Gd-DTPA at a dose of 15–20 mL was used as the contrast agent for dynamic contrast enhancement and injected into the dorsal vein of the hand at 2–2.5 mL/s using a high-pressure syringe. DCE MR images were obtained in the AP (18–25 s) and PVP (45–60 s) after injection of the contrast agent.

Sequence	TR/TE (ms)	FA (°)	Matrix (mm²)	FOV (mm ²)	ST (mm)
BH Ax LAVA-Flex	4/2	12	260×192	$320 \times 320 - 360 \times 360$	2.6
RTr Ax fs T ₂ WI	2609/97	110	384×384	$320 \times 320 - 380 \times 380$	5
BH Ax LAVA-Flex+C	4/2	12	224×192	$320 \times 320 - 360 \times 360$	5

Table 1. MRI sequence and parameters.

Notes: TR, repetition time; TE, echo time; FA, flip angle; FOV, field of view; ST, section thickness; LAVA-Flex, liver acquisition with volume acceleration flexible.

2.3. Image Segmentation and Feature Extraction

The MR images of the patients in the FS- T_2 WI and AP as well as PVP were exported in digital imaging and communications in medicine (DICOM) format and imported into IBEX software (β 1.0, https://sourceforge.net/projects/ibex-mda/, accessed on 13 November 2021) for tumor image segmentation. Without knowing the pathological results, an observer with 6 years of experience in abdominal radiology used the IBEX software to delineate the region of interest (ROI) along the edge of the lesion that contained the tumor layer by layer,

Cancers 2023, 15, 5373 4 of 17

and the entire tumor volume was manually delineated (Figure 2). After segmenting the MR images, the gray-level run-length matrix (GLRLM), gray-level cooccurrence matrix (GLCM), intensity histogram and shape features were extracted and used to construct the FS-T₂WI, AP and PVP datasets.

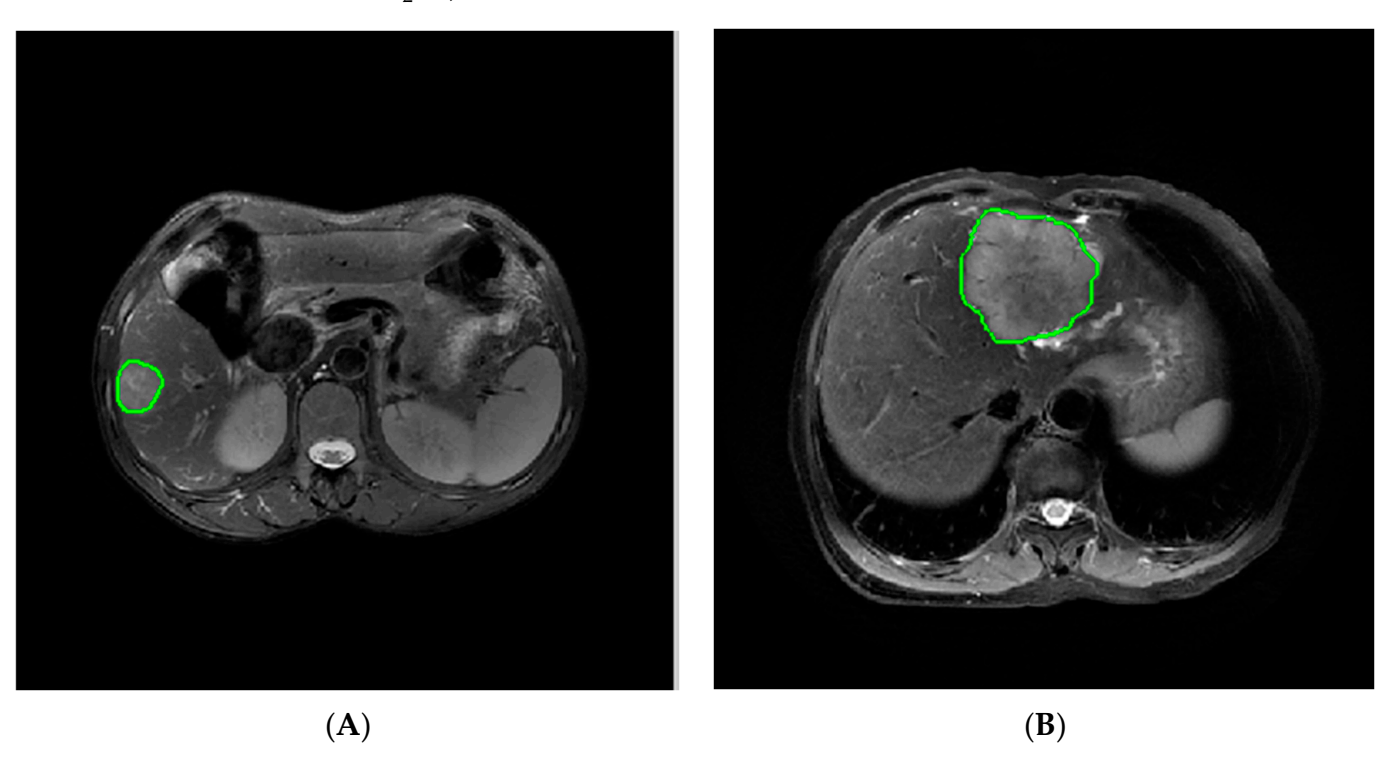


Figure 2. Delineation of the ROI along the edge of the lesion: (**A**) ROI segmentation on FS-T₂WI in the case of HCC and (**B**) ICC, respectively.

2.4. Feature Selection

Altogether, 61 patients (42 with HCC and 19 with ICC) were randomly selected for intra- and intergroup consistency analysis. Interobserver consistency was assessed by comparing the segmentation results of two radiologists (observers 1 and 2, with 5 and 6 years of experience, respectively). Intraobserver consistency was assessed by comparing the segmentation results obtained by observer 2 more than one week after the initial results were obtained. The intraclass correlation coefficient was used to assess interobserver consistency, with a coefficient \geq 0.75 being considered to indicate good consistency. To eliminate discrepancies in the index dimension, all data were standardized via Z-score normalization. The dataset generated by each sequence was subjected to intra- and interobserver consistency tests. Features with an intraclass correlation coefficient <0.75 were eliminated.

From the stable features that remained, features that significantly differentiated HCC from ICC were selected using one-way statistical analysis (independent-samples t test or Mann–Whitney U test, according to the characteristics of the data distribution) (p < 0.05). To avoid overfitting, least absolute shrinkage and selection operator (LASSO) regression analysis was performed to select the core radiomics features in differentiating HCC from ICC. The regularization parameter (λ) of the selected features was adjusted with 10-fold cross-validation using the 1-standard-error (1-SE) method.

2.5. Model Establishment and Evaluation

The optimal radiomics features selected from each sequence were used to establish radiomics models (FS- T_2 WI, AP and PVP models), and clinical variables were used to establish the clinical model (C model) with logistic regression. By integrating the optimal radiomic features from each model, a joint radiomics model (JR model) was established [45]. Finally, the optimal radiomics features and clinical risk factors were combined to establish

Cancers 2023, 15, 5373 5 of 17

the radiomics–clinical model (RC model). The efficacy of the models was assessed considering the area under the receiver operating characteristic (ROC) curve (AUC), sensitivity, specificity, positive predictive value (PPV), negative predictive value (NPV), accuracy and F1 score as determined from the logistic regression confusion matrix.

2.6. Statistical Methods

R software (4.1.2, https://www.r-project.org/, accessed on 8 December 2021) was used for statistical data processing. Specifically, the software packages "psych", "glmnet" and "pROC" were used to assess the intra- and intergroup consistency in the radiomics features to perform LASSO regression analysis and to plot the ROC curves, respectively. The normality and homogeneity of variance of the quantitative data were tested using the Shapiro–Wilk test and Bartlett test, respectively. The independent-samples t test was performed for quantitative data with a normal distribution and homogeneous variance; otherwise, the Mann–Whitney U test was performed. Quantitative data are presented as the means or medians. Categorical variables were analyzed using the chi-square test and are presented as percentages. Two-sided p values < 0.05 were considered to indicate statistical significance.

3. Results

3.1. Patient Characteristics

Among the 177 patients, 129 had HCC (112 men and 17 women) and 48 had ICC (19 men and 29 women). Cirrhosis occurred in 121 patients (107 with HCC and 14 with ICC), and multinodular liver cancer occurred in 65 patients (47 with HCC and 18 with ICC). The maximum tumor diameter was 6.57 \pm 3.22 cm (Table 2). The HCC and ICC groups demonstrated significant differences in gender, serum AFP and extrahepatic metastasis status.

Table 2.	Dations	اممناه	alaamaa	Louisties
Table 2.	Patient	clinical	charac	teristics.

Parameter	Training Cohort (n = 124)	Validation Cohort (n = 53)	p Value
Sex			
Male	94	38	0.565
Female	30	15	
Age			
≤ 6 0	78	32	0.751
>60	46	21	
Satellite nodules			
Yes	47	18	0.618
No	77	35	
Diameter			
≤ 5	41	25	0.076
>5	83	28	
Ascites			
Yes	36	18	0.514
No	88	35	
Hemorrhagic necrosis			
Yes	86	31	0.162
No	38	22	
Pseudocapsule			
Yes	26	11	0.975
No	98	42	

Cancers 2023, 15, 5373 6 of 17

Table 2. Cont.

Parameter	Training Cohort (n = 124)	Validation Cohort (n = 53)	p Value	
Extrahepatic				
metastases			0.224	
Yes	23	6	0.234	
No	101	47		
Portal vein tumor				
thrombus			0.445	
Yes	35	18	0.445	
No	89	35		
Cirrhosis				
Yes	83	38	0.533	
No	41	15		
Hepatitis B or C				
Yes	90	39	0.891	
No	34	14		
AFP (ng/mL)				
<20	54	30	0.250	
20~400	21	8	0.259	
>400	49	15		
DCP (mAU/mL)				
≤27.8	11	5	0.905	
>27.8	113	48		
CA19-9 (U/mL)				
≤37	68	24	0.244	
>37	56	29		
CEA (μg/L)				
<u>≤</u> 5	80	32	0.601	
_ >5	44	21		
Histologic result				
HČC	90	39	0.891	
ICC	34	14		

Notes: HCC, hepatocellular carcinoma; ICC, intrahepatic cholangiocarcinoma; AFP, alpha-fetoprotein; CA19-9, carbohydrate antigen 19-9; DCP, des-gamma-carboxy prothrombin; CEA, carcinoembryonic antigen.

3.2. Feature Extraction and Selection

A total of 352 features were extracted from each of the FS- T_2 WI, AP and PVP datasets. Features with intra- and intergroup intraclass correlation coefficients <0.75 were eliminated, and the remaining features were further analyzed (Figure 3).

There were 327, 331 and 319 significantly different features in the FS- T_2 WI, AP and PVP datasets, respectively (p < 0.05), according to the independent-samples t test or Mann–Whitney U test. Finally, one, six and four optimal features, respectively, from these datasets were selected in LASSO regression (Figure 4 and Table 3).

Cancers 2023, 15, 5373 7 of 17

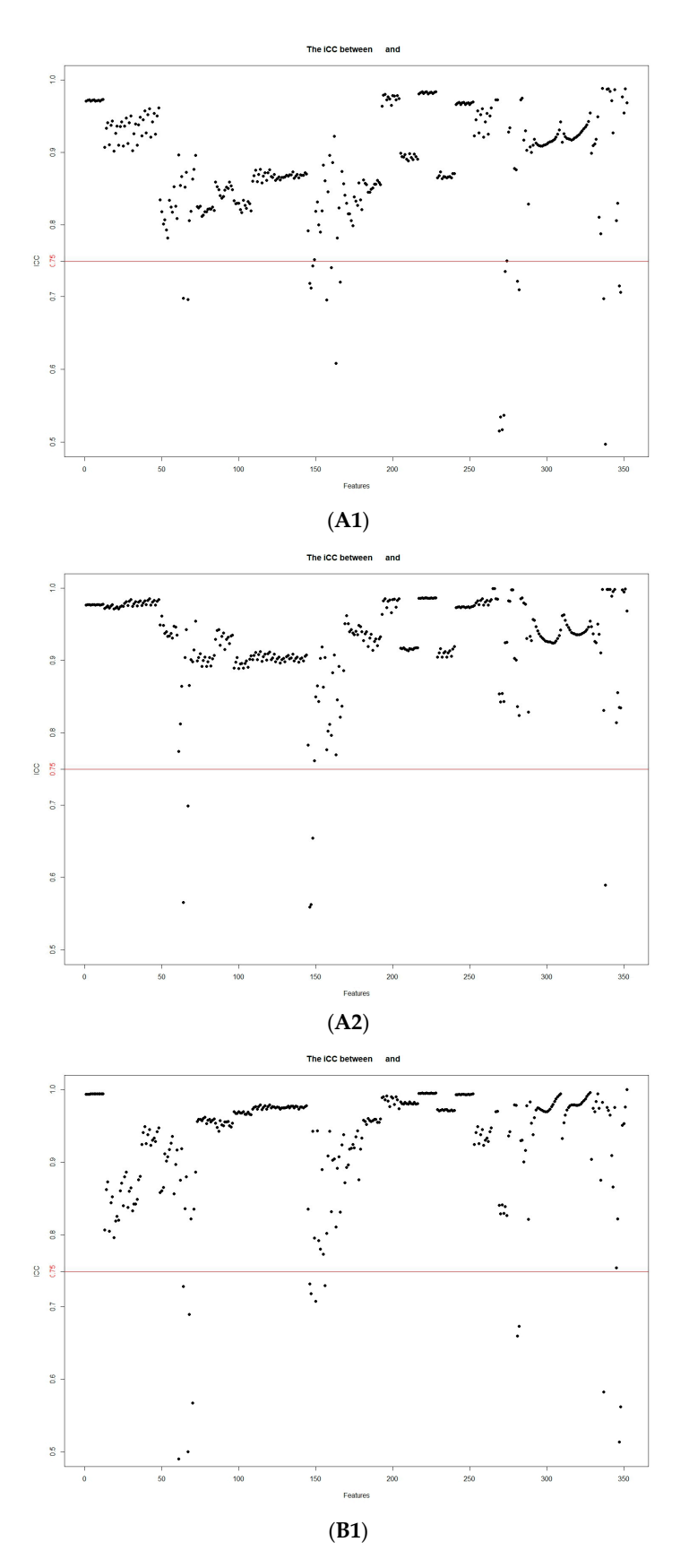


Figure 3. Cont.

Cancers 2023, 15, 5373 8 of 17

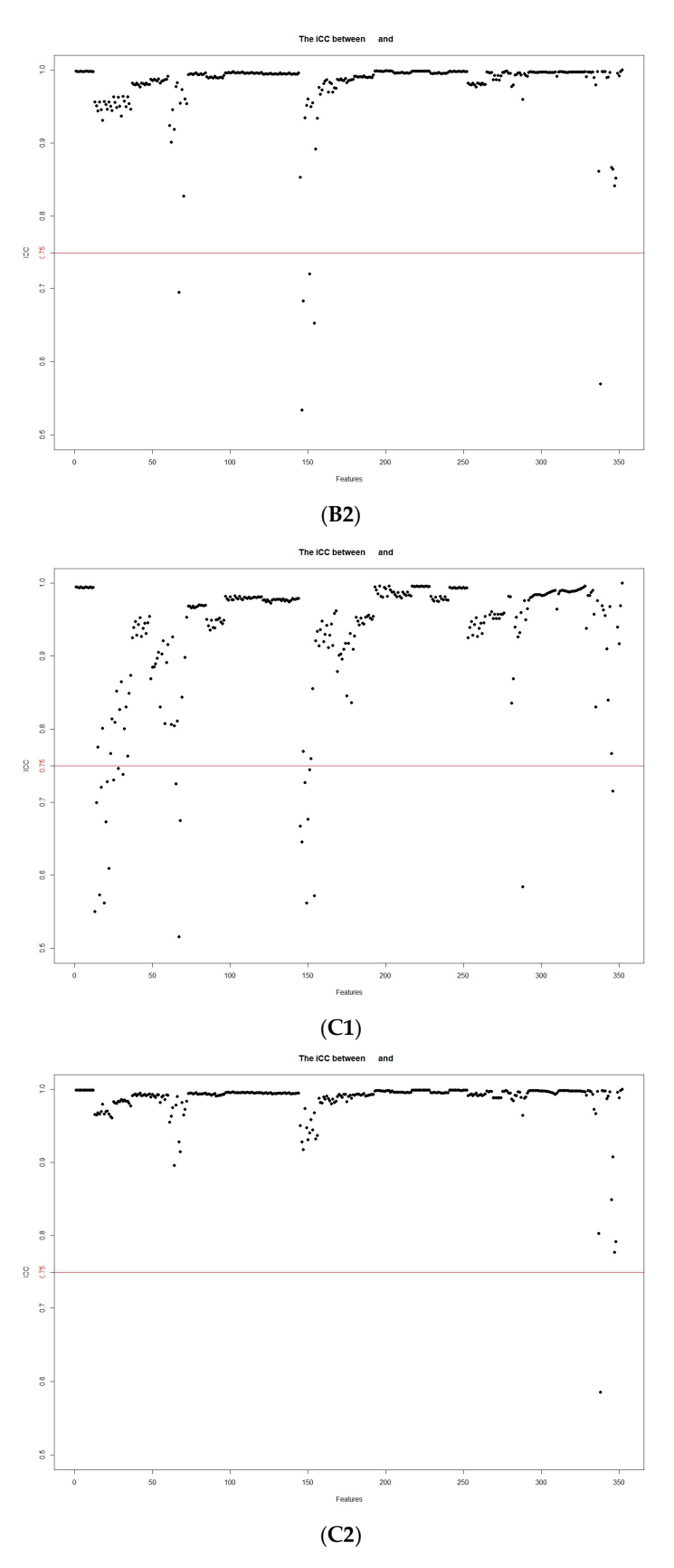


Figure 3. Stability assessment of the extracted MRI radiomic features according to inter- and intraobserver intraclass correlation coefficients: **(A1)** intergroup FS-T₂WI; **(A2)** intragroup FS-T₂WI; **(B1)** intergroup arterial phase; **(B2)** intragroup arterial phase; **(C1)** intergroup portal venous phase; **(C2)** intragroup portal venous phase.

Cancers 2023, 15, 5373 9 of 17

Table 3. Radiomics features identifying HCC and ICC selected from each dataset in LASSO regression.

Cohort	Feature Type	Feature Name		
FS-T ₂ WI	Shape features $(n = 1)$	Roundness		
	Texture features $(n = 3)$			
	GLCM (n = 1)	45-7InverseDiffMomentNorm		
Arterial phase	GLRLM $(n = 2)$	0LongRunEmphasis 90ShortRunLowGrayLevelEmpha		
1	Intensity histogram features $(n = 1)$	InterOuartileRange		
		Mass		
	Shape features $(n = 2)$	Roundness		
	Texture features (n = 2)			
D (1 1	GLCM(n = 2)	90-1Contrast		
Portal venous phase	,	45-7InverseDiffMomentNorm		
	Intensity histogram features $(n = 2)$	InterQuartileRange		
	,	MeanAbsoluteDeviation		

Notes: HCC, hepatocellular carcinoma; ICC, intrahepatic cholangiocarcinoma; FS-T₂WI, fat suppression T₂-weighted imaging; GLCM, gray-level cooccurrence matrix; GLRLM, gray-level run-length matrix. GLCM features were constructed in four directions ($\theta = 0^{\circ}$, 45° , 90° and 135°) and three offsets (d = 1, 4 and 7); GLRLM features were constructed in two directions ($\theta = 0^{\circ}$, 90°) and one offset (d = 1).

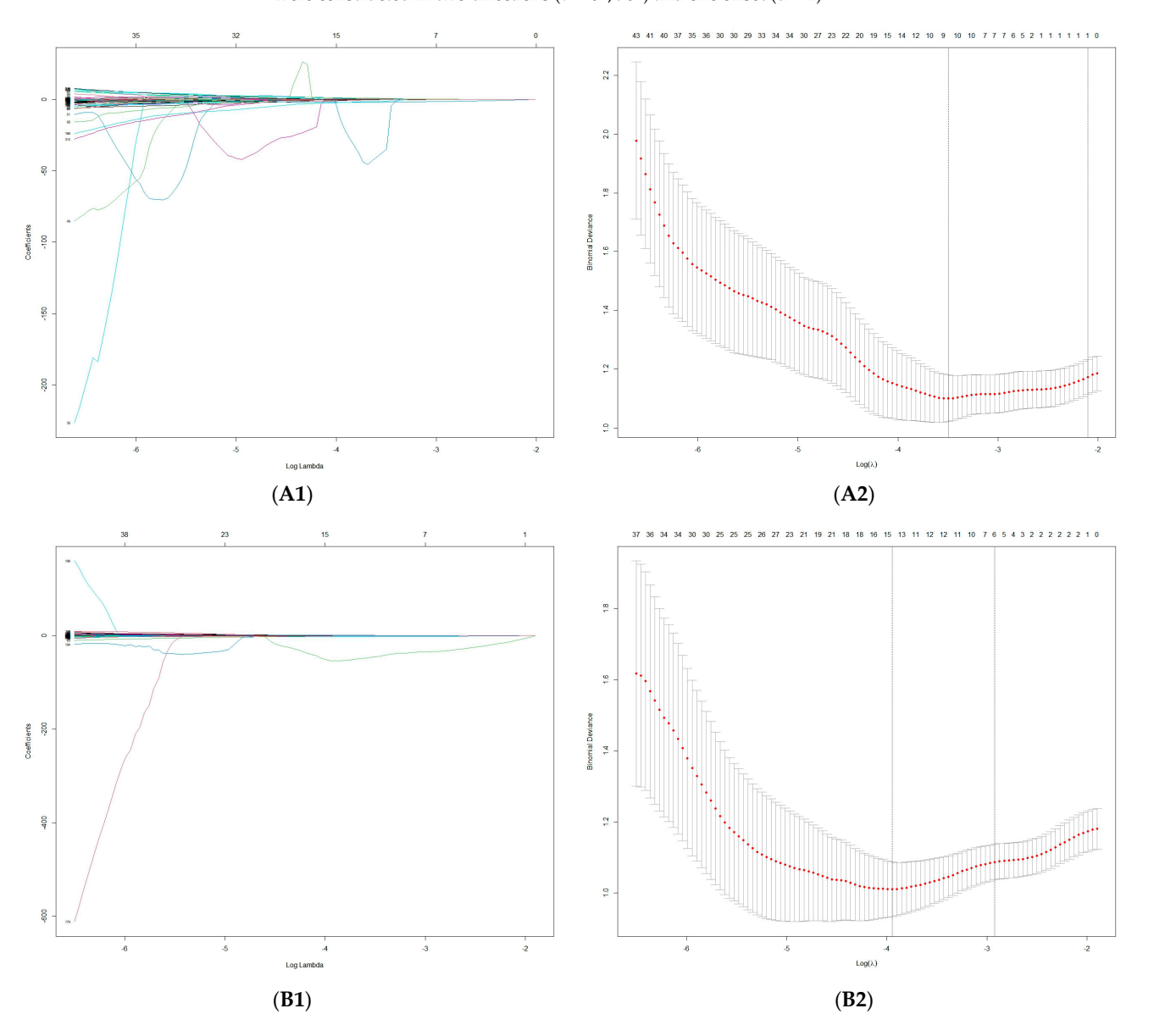


Figure 4. Cont.

Cancers 2023, 15, 5373 10 of 17

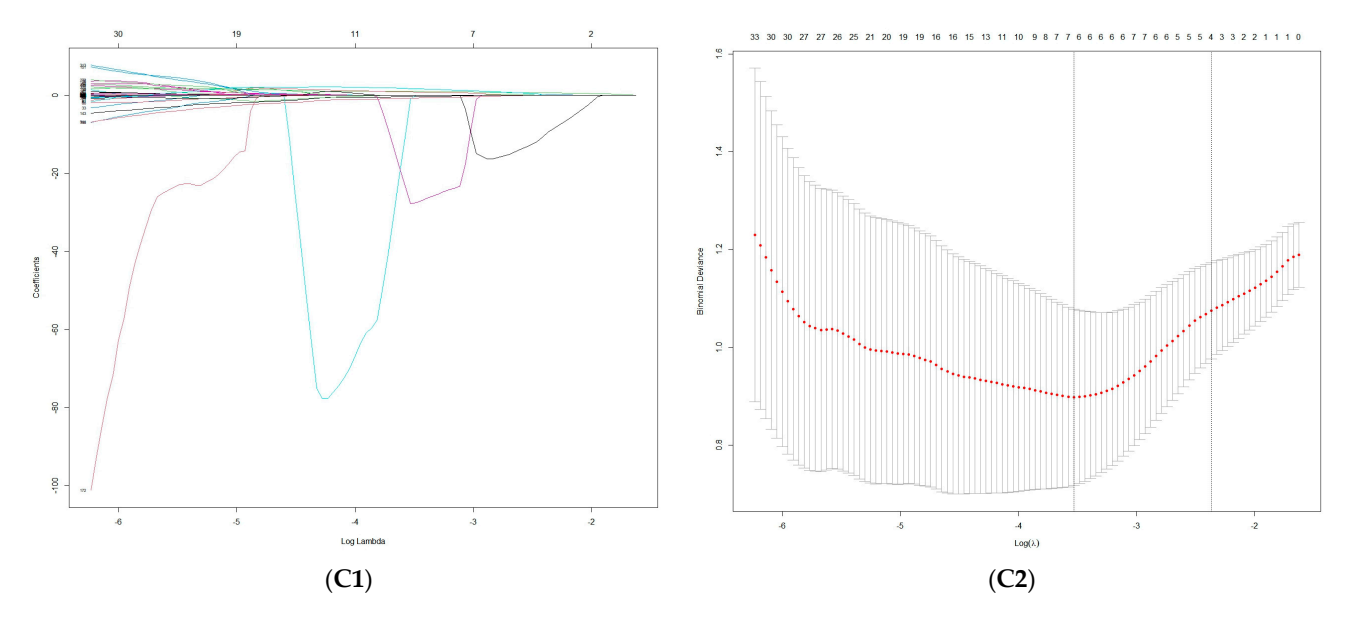


Figure 4. Feature selection using LASSO. (**A1–C1**) LASSO coefficient profiles of the radiomics features in the FS-T₂WI, arterial phase and portal venous phase; (**A2–C2**) mean square error path using 10-fold cross-validation in the FS-T₂WI, arterial phase and portal venous phase, respectively.

3.3. Model Evaluation

The AUCs of the FS- T_2 WI, AP, PVP, JR, C and RC models for distinguishing HCC from ICC were 0.693, 0.863, 0.818, 0.914, 0.936 and 0.977 in the training group and 0.690, 0.784, 0.727,0.802, 0.860 and 0.877 in the validation group, respectively (Table 4 and Figure 5).

Cohort	Model	AUC	Sen	Spe	PPV	NPV	ACC	F1 Score
	FS-T ₂ WI model	0.693	0.147	0.956	0.556	0.748	0.734	0.233
Training	AP model	0.863	0.588	0.933	0.769	0.857	0.839	0.667
	PVP model	0.818	0.588	0.922	0.741	0.856	0.831	0.656
	JR model	0.914	0.706	0.922	0.774	0.892	0.863	0.738
	C model	0.936	0.706	0.978	0.923	0.898	0.903	0.800
	RC model	0.977	0.853	0.978	0.935	0.946	0.944	0.892
Validation	FS-T ₂ WI model	0.690	0.071	0.974	0.5	0.745	0.736	0.125
	AP model	0.784	0.571	0.897	0.667	0.854	0.811	0.615
	PVP model	0.727	0.357	0.897	0.556	0.795	0.756	0.435
	JR model	0.802	0.571	0.923	0.727	0.857	0.83	0.640
	C model	0.860	0.714	0.949	0.833	0.902	0.887	0.769
	RC model	0.877	0.714	0.897	0.714	0.897	0.849	0.714

Table 4. Efficacy of each model in identifying HCC and ICC.

Notes: HCC, hepatocellular carcinoma; ICC, intrahepatic cholangiocarcinoma; FS-T₂WI, fat suppression T₂-weighted imaging; AP, arterial phase; PVP, portal venous phase; JR, joint radiomic; C, clinical; RC, radiomics-clinical; AUC, area under the receiver operating characteristic curve; ACC, accuracy; Sen, sensitivity; Spe, specificity; PPV, positive predictive value; NPV, negative predictive value.

Cancers 2023, 15, 5373 11 of 17

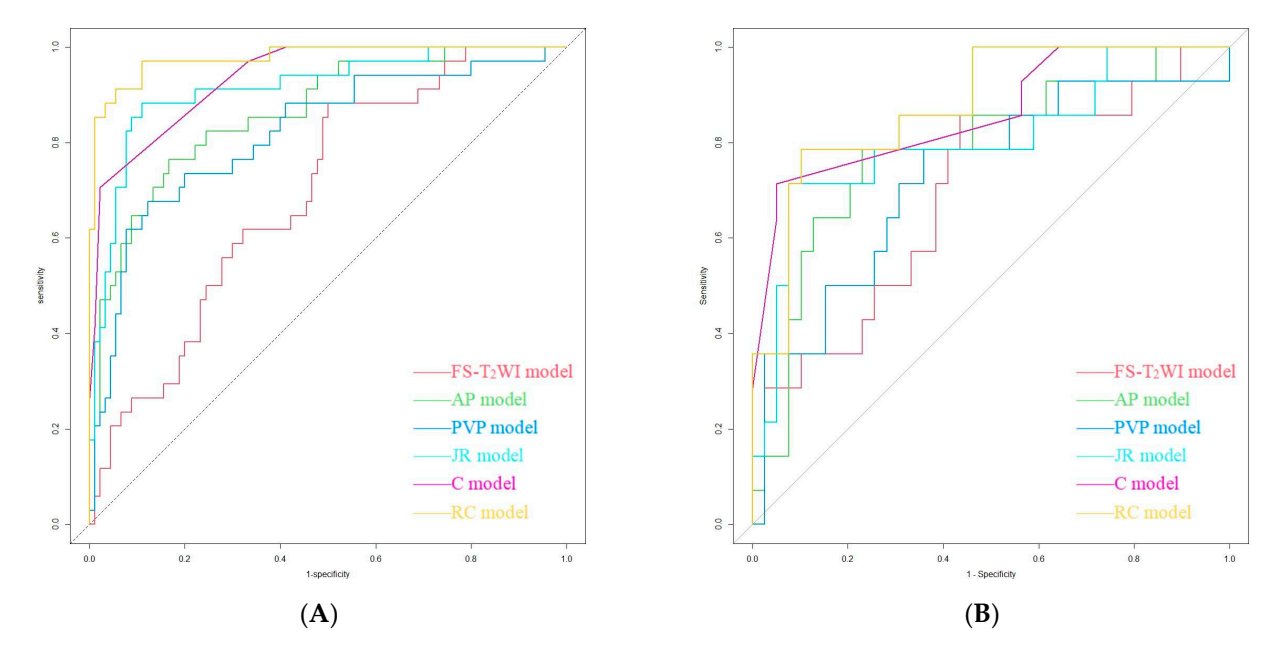


Figure 5. Performance of the FS-T₂WI model, AP model, PVP model, JR model, C model and RC model in identifying HCC and ICC in the training group (**A**) and validation group (**B**) as detected using ROC curve analysis.

4. Discussion

MRI is characterized by high soft-tissue contrast, multiparametric and multidirectional imaging and a lack of radiation, making it the preferred imaging method for identifying and diagnosing liver nodules [57,58]. Dynamic-contrast-enhanced MRI (DCE-MRI) is superior to dynamic-contrast-enhanced CT in the detection and diagnosis of small HCC lesions (maximum diameter ≤ 2.0 cm) [59,60]. Typical HCC displays significant heterogeneous enhancement in the arterial phase on DCE-MRI and reduced enhancement in the portal and/or parenchymal phase relative to that of normal liver parenchyma, resulting in a "fast-in and fast-out" enhancement pattern [25,28]. In contrast, ICC shows less obvious enhancement or mild heterogeneous enhancement in the arterial phase on DCE-MRI that gradually increases with time [26,27]. However, it is still difficult to differentiate HCC from ICC in clinical practice. Studies [30,34–36] have shown that small ICC lesions (diameter < 3 cm) and some ICC lesions in the setting of cirrhosis (approximately 7%) show the same enhancement pattern as typical HCC lesions, and approximately 10–20% of HCC lesions (especially small, hypovascular or sclerosing HCC lesions) show less obvious enhancement on imaging.

Choi et al. [61] conducted gadoxetic-acid-enhanced MR and dynamic CT scans to identify HCC and ICC. The results showed that PVP washout instead of conventional washout in gadoxetic-acid-enhanced MRI can prevent the misidentification of HCC as ICC in patients with cirrhosis; however, it reduces the sensitivity of the method for identifying HCC. Diffusion-weighted imaging (DWI) reflects the diffusion of water molecules in tissues by measuring the apparent diffusion coefficient (ADC). Wei et al. [62] and Lewis et al. [63] found that the ADC can help differentiate HCC from ICC. However, ICC has multiple cellular origins and shares similar biological behaviors with HCC to some extent; thus, the ADC of ICC can partially overlap with that of HCC. Additionally, DWI does not display small lesions well because of the limited spatial resolution, and conventional DWI is based on a monoexponential model that cannot differentiate between water molecule diffusion and blood perfusion [64]. Intravoxel incoherent motion-DWI (IVIM-DWI) can simultaneously quantify the diffusion of water molecules and microcirculatory perfusion in living tissues. A previous study [65] showed that both the ADC and D_{slow} values were significantly lower in HCC than in ICC, but the D_{fast} value was significantly higher in HCC than in ICC; furthermore, D_{fast} was more efficient in the differential diagnosis of

Cancers 2023, 15, 5373 12 of 17

HCC and ICC, and there was no significant difference in the f value between D_{fast} and D_{slow} . The value of IVIM-DWI in identifying HCC and ICC has also been reported by other scholars [62,66,67]. However, the conclusion regarding D_{fast} and f in distinguishing HCC from ICC remains inconsistent or controversial; thus, further research is needed. As an effective tumor imaging tool, positron emission tomography (PET)-MRI can play a role in patient management. Çelebi et al. [68] argued that PET-MRI using ¹⁸F-fluorodeoxyglucos (¹⁸F-FDG) as a tracer agent can help differentiate between HCC and ICC. However, there is a need to deeply explore whether there are substantial differences in FDG uptake between HCC and ICC, the accuracy of identification in certain challenging cases (e.g., specific subgroups of patients in which the standard uptake value (SUV) is not a determining factor) and the optimal imaging sequence and model.

To date, few studies have investigated the differentiation of HCC from ICC based on MRI radiomics [42,44,63,69]. Liu et al. [44] adopted machine-learning-based CT and MR image features in the identification of cHCC-CC, ICC and HCC. The results showed that MRI features had the highest efficacy in differentiating between cHCC-CC and non-cHCC-CC, while CT features were less valuable. Moreover, precontrast- and portal-phase CT features were superior to enhanced MRI features in differentiating between HCC and non-HCC (AUC = 0.79–0.81 for MRI, 0.81 for precontrast-phase CT and 0.71 for portal-phase CT). Wang et al. [69] used MRI radiomics to preoperatively identify cHCC-CC, HCC and ICC and found that the performance of the higher-order feature-based model exceeded that of the lower-order feature-based model by approximately 10% and that the former performed better in identifying HCC in the delayed phase. Lewis et al. [63] extracted first-order radiomics features from ADC data and evaluated the ability of these features and the Liver Imaging Reporting and Data System (LI-RADS) classification to differentiate HCC, ICC and cHCC-CC. The results revealed that the AUCs of the combination of sex, LI-RADS grade and the fifth percentile of the ADC in diagnosing HCC were 0.90 and 0.89 for two independent observers, respectively. T₂*WI can reflect the magnetic susceptibility variation in tissues and thus be used to assess the biological properties of tumor tissues [70]. Huang et al. [42] extracted radiomic features from T2*W images and then established radiomic nomogram models combined with clinical risk factors to distinguish between HCC and ICC. The results showed that the AUCs of the radiomics model were 0.90 and 0.91 in the training and validation groups, respectively, the AUCs of the clinical features were 0.88 in the training group and 0.83 in the validation group, and the AUCs of the radiomics nomogram were 0.97 and 0.95 in the training and validation groups, respectively. Similar results were obtained by Zhou et al. [43]. However, the efficacy of a joint model incorporating multiple sequence features was not investigated in these studies.

Different kinds of information related to tumor structure can be revealed by different sequences: T₂WI exhibits the underlying tumor morphology and heterogeneity, and enhanced scans can reflect differences in the tumor blood supply. In this work, enhancements in the arterial and venous phases were combined based on T₂WI to explore the efficacy of a joint model according to the blood supply status and enhancement patterns of HCC and ICC. The results showed that while each model had the potential to identify HCC and ICC in both the training and validation groups, the joint model incorporating multiple sequence features showed the highest efficacy [44,69]. Radiomics features based on MRI in combination with clinical risk factors are valuable for liver tumor differentiation [71]. In this study, univariate and multivariate analyses indicated that gender, serum AFP and extrahepatic metastasis status were independent clinical risk factors. The model integrating the radiomics features and clinical risk factors showed a further improvement in performance. The AUC of the T₂WI model was relatively low in this study, consistent with the findings of Liu et al. [72]. Therefore, the value of FS-T₂WI-based radiomics in distinguishing between HCC and ICC remains to be properly determined with further research.

In this study, we used the LASSO for feature selection. The LASSO is a well-known regularization technique which is popularly used in radiomics studies. One of the most unique advantages of this technique is that it reduces overfitting without limiting a subset

Cancers 2023, 15, 5373 13 of 17

of the dataset to only be used for internal validation. However, the LASSO does not eliminate the need to validate models in external datasets. A corresponding important disadvantage of the LASSO method is that the regression coefficients may not be reliably interpretable in terms of independent risk factors, as its focus is on the prediction of the optimal combination, rather than the accuracy of the estimation and interpretation of the contribution of individual variables [73]. The radiomics features selected were mainly GLCM and GLRLM features, textural features used to quantify tumor heterogeneity by reflecting the relationship between adjacent voxels/pixels [74], which is consistent with the results of several related studies [42,44,75–80]. Histogram features show the global distribution of grayscale values in the image and can also be used to assess tumor heterogeneity [81]. Lewis et al. [63] found that the 5th/10th/95th percentiles of the ADC could significantly differentiate HCC from ICC and cHCC-CC. Shape features reflect the geometric characteristics of tumors [74]; Zhao et al. [82] confirmed that HCC tends to be more spherical than ICC in terms of morphology.

This study had the following limitations. (1) In this retrospective study, many HCC and ICC patients who did not undergo pretherapeutic MRI scans were excluded, so there may be a potential selection bias. (2) The sample was small and from a single center, and cHCC-CC and ICC types other than the mass-forming type were not included in the study. In the future, the sample size should be expanded to multiple centers for further external validation. (3) Other relevant MRI sequences were not analyzed, so their potential contributions might have been ignored.

5. Conclusions

Multisequence MRI radiomics models can be used to pretherapeutically distinguish between HCC and ICC; the combined model integrating the optimal radiomic features with clinical risk factors can further improve the identification performance.

Author Contributions: N.L. and L.Y. wrote the paper. Y.W., Y.T. and J.Z. collected the data. X.H., L.Y. and X.Z. designed the research. All authors have read and agreed to the published version of the manuscript.

Funding: This work was supported by the Project of City-University Science and Technology Strategic Cooperation of Nanchong City (No. 20SXQT0324).

Institutional Review Board Statement: This study was conducted in accordance with the Declaration of Helsinki and approved by the Ethics Committee of the Affiliated Hospital of North Sichuan Medical College (No. 2022ER545-1).

Informed Consent Statement: The requirement for patient consent was waived due to the retrospective nature of anonymous data collection without any risk to patients.

Data Availability Statement: The data presented in this study are available upon request from the corresponding author.

Conflicts of Interest: The authors declare no conflict of interest.

References

- Sung, H.; Ferlay, J.; Siegel, R.L.; Laversanne, M.; Soerjomataram, I.; Jemal, A.; Bray, F. Global Cancer Statistics 2020: GLOBOCAN
 Estimates of Incidence and Mortality Worldwide for 36 Cancers in 185 Countries. CA Cancer J. Clin. 2021, 71, 209–249. [CrossRef]
 [PubMed]
- 2. Si, Y.Q.; Wang, X.Q.; Pan, C.C.; Wang, Y.; Lu, Z.M. An Efficient Nomogram for Discriminating Intrahepatic Cholangiocarcinoma From Hepatocellular Carcinoma: A Retrospective Study. *Front. Oncol.* **2022**, *12*, 833999. [CrossRef] [PubMed]
- 3. Cheng, N.; Khoo, N.; Chung, A.Y.F.; Goh, B.K.P.; Cheow, P.C.; Chow, P.K.H.; Lee, S.Y.; Ooi, L.L.; Jeyaraj, P.R.; Kam, J.H.; et al. Pre-operative Imaging Characteristics in Histology-Proven Resected Intrahepatic Cholangiocarcinoma. *World J. Surg.* 2020, 44, 3862–3867. [CrossRef] [PubMed]
- 4. Florio, A.A.; Ferlay, J.; Znaor, A.; Ruggieri, D.; Alvarez, C.S.; Laversanne, M.; Bray, F.; McGlynn, K.A.; Petrick, J.L. Global trends in intrahepatic and extrahepatic cholangiocarcinoma incidence from 1993 to 2012. *Cancer* 2020, 126, 2666–2678. [CrossRef] [PubMed]
- 5. Saha, S.K.; Zhu, A.X.; Fuchs, C.S.; Brooks, G.A. Forty-Year Trends in Cholangiocarcinoma Incidence in the U.S.: Intrahepatic Disease on the Rise. *Oncologist* **2016**, *21*, 594–599. [CrossRef]

Cancers 2023, 15, 5373 14 of 17

6. Valle, J.W.; Borbath, I.; Khan, S.A.; Huguet, F.; Gruenberger, T.; Arnold, D.; ESMO Guidelines Committee. Biliary cancer: ESMO Clinical Practice Guidelines for diagnosis, treatment and follow-up. *Ann. Oncol.* **2016**, 27 (Suppl. S5), v28–v37. [CrossRef]

- 7. Banales, J.M.; Cardinale, V.; Carpino, G.; Marzioni, M.; Andersen, J.B.; Invernizzi, P.; Lind, G.E.; Folseraas, T.; Forbes, S.J.; Fouassier, L.; et al. Expert consensus document: Cholangiocarcinoma: Current knowledge and future perspectives consensus statement from the European Network for the Study of Cholangiocarcinoma (ENS-CCA). *Nat. Rev. Gastroenterol. Hepatol.* **2016**, 13, 261–280. [CrossRef]
- 8. Gupta, A.; Dixon, E. Epidemiology and risk factors: Intrahepatic cholangiocarcinoma. *Hepatobiliary Surg. Nutr.* **2017**, *6*, 101–104. [CrossRef]
- 9. Nart, D.; Ertan, Y.; Pala, E.E.; Zeytunlu, M.; Kilic, M.; Yilmaz, F. Intrahepatic cholangiocarcinoma arising in chronic viral hepatitis-associated cirrhosis: Two transplant cases. *Transplant. Proc.* **2008**, *40*, 3813–3815. [CrossRef]
- 10. Kelley, R.K.; Bridgewater, J.; Gores, G.J.; Zhu, A.X. Systemic therapies for intrahepatic cholangiocarcinoma. *J. Hepatol.* **2020**, 72, 353–363. [CrossRef]
- 11. Banales, J.M.; Iñarrairaegui, M.; Arbelaiz, A.; Milkiewicz, P.; Muntané, J.; Muñoz-Bellvis, L.; La Casta, A.; Gonzalez, L.M.; Arretxe, E.; Alonso, C.; et al. Serum Metabolites as Diagnostic Biomarkers for Cholangiocarcinoma, Hepatocellular Carcinoma, and Primary Sclerosing Cholangitis. *Hepatology* **2019**, *70*, 547–562. [CrossRef] [PubMed]
- 12. Buettner, S.; van Vugt, J.L.; IJzermans, J.N.; Groot Koerkamp, B. Intrahepatic cholangiocarcinoma: Current perspectives. *Onco Targets Ther.* **2017**, *10*, 1131–1142. [CrossRef] [PubMed]
- 13. Liu, W.; Wang, K.; Bao, Q.; Sun, Y.; Xing, B.C. Hepatic resection provided long-term survival for patients with intermediate and advanced-stage resectable hepatocellular carcinoma. *World J. Surg. Oncol.* **2016**, *14*, 62. [CrossRef]
- 14. Weber, S.M.; Ribero, D.; O'Reilly, E.M.; Kokudo, N.; Miyazaki, M.; Pawlik, T.M. Intrahepatic cholangiocarcinoma: Expert consensus statement. *HPB* **2015**, *17*, 669–680. [CrossRef] [PubMed]
- 15. Spolverato, G.; Kim, Y.; Alexandrescu, S.; Popescu, I.; Marques, H.P.; Aldrighetti, L.; Clark Gamblin, T.; Miura, J.; Maithel, S.K.; Squires, M.H.; et al. Is Hepatic Resection for Large or Multifocal Intrahepatic Cholangiocarcinoma Justified? Results from a Multi-Institutional Collaboration. *Ann. Surg. Oncol.* **2015**, 22, 2218–2225. [CrossRef]
- 16. Bruix, J.; Reig, M.; Sherman, M. Evidence-Based Diagnosis, Staging, and Treatment of Patients With Hepatocellular Carcinoma. *Gastroenterology* **2016**, *150*, 835–853. [CrossRef]
- 17. Moris, D.; Palta, M.; Kim, C.; Allen, P.J.; Morse, M.A.; Lidsky, M.E. Advances in the treatment of intrahepatic cholangiocarcinoma: An overview of the current and future therapeutic landscape for clinicians. *CA Cancer J. Clin.* **2023**, 73, 198–222. [CrossRef]
- 18. Lee, S.M.; Lee, J.M.; Ahn, S.J.; Kang, H.J.; Yang, H.K.; Yoon, J.H. LI-RADS Version 2017 versus Version 2018: Diagnosis of Hepatocellular Carcinoma on Gadoxetate Disodium-enhanced MRI. *Radiology* **2019**, 292, 655–663. [CrossRef]
- 19. Liu, X.; Ni, X.; Li, Y.; Yang, C.; Wang, Y.; Ma, C.; Zhou, C.; Lu, X. Diagnostic Performance of LI-RADS Version 2018 for Primary Liver Cancer in Patients With Liver Cirrhosis on Enhanced MRI. *Front. Oncol.* **2022**, *12*, 934045. [CrossRef]
- 20. Feng, M.; Pan, Y.; Kong, R.; Shu, S. Therapy of Primary Liver Cancer. Innovation 2020, 1, 100032. [CrossRef]
- Huang, D.; Lin, Q.; Song, J.; Xu, B. Prognostic Value of Pretreatment Serum CA199 in Patients with Locally Advanced Rectal Cancer Treated with CRT Followed by TME with Normal Pretreatment Carcinoembryonic Antigen Levels. *Dig. Surg.* 2021, 38, 24–29. [CrossRef] [PubMed]
- 22. Qi, F.; Zhou, A.; Yan, L.; Yuan, X.; Wang, D.; Chang, R.; Zhang, Y.; Shi, F.; Han, X.; Hou, J.; et al. The diagnostic value of PIVKA-II, AFP, AFP-L3, CEA, and their combinations in primary and metastatic hepatocellular carcinoma. *J. Clin. Lab. Anal.* 2020, 34, e23158. [CrossRef] [PubMed]
- 23. Afshar, M.; Fletcher, P.; Bardoli, A.D.; Ma, Y.T.; Punia, P. Non-secretion of AFP and neutrophil lymphocyte ratio as predictors for survival in hepatocellular carcinoma patients treated with sorafenib: A large UK cohort. *Oncotarget* **2018**, *9*, 16988–16995. [CrossRef] [PubMed]
- 24. Teng, D.; Wu, K.; Sun, Y.; Zhang, M.; Wang, D.; Wu, J.; Yin, T.; Gong, W.; Ding, Y.; Xiao, W.; et al. Significant increased CA199 levels in acute pancreatitis patients predicts the presence of pancreatic cancer. *Oncotarget* **2018**, *9*, 12745–12753. [CrossRef] [PubMed]
- Marrero, J.A.; Kulik, L.M.; Sirlin, C.B.; Zhu, A.X.; Finn, R.S.; Abecassis, M.M.; Roberts, L.R.; Heimbach, J.K. Diagnosis, Staging, and Management of Hepatocellular Carcinoma: 2018 Practice Guidance by the American Association for the Study of Liver Diseases. Hepatology 2018, 68, 723–750. [CrossRef] [PubMed]
- 26. Lafaro, K.J.; Cosgrove, D.; Geschwind, J.F.; Kamel, I.; Herman, J.M.; Pawlik, T.M. Multidisciplinary Care of Patients with Intrahepatic Cholangiocarcinoma: Updates in Management. *Gastroenterol. Res. Pract.* **2015**, 2015, 860861. [CrossRef]
- 27. Hennedige, T.P.; Neo, W.T.; Venkatesh, S.K. Imaging of malignancies of the biliary tract—An update. *Cancer Imaging* **2014**, *14*, 14. [CrossRef]
- European Association for Study of Liver; European Organisation for Research and Treatment of Cancer. European Organisation
 For Research And Treatment Of Cancer. EASL-EORTC clinical practice guidelines: Management of hepatocellular carcinoma. J.
 Hepatol. 2012, 56, 908–943. [CrossRef]
- 29. Li, R.; Cai, P.; Ma, K.S.; Ding, S.Y.; Guo, D.Y.; Yan, X.C. Dynamic enhancement patterns of intrahepatic cholangiocarcinoma in cirrhosis on contrast-enhanced computed tomography: Risk of misdiagnosis as hepatocellular carcinoma. *Sci. Rep.* **2016**, *6*, 26772. [CrossRef]

Cancers 2023, 15, 5373 15 of 17

30. Huang, B.; Wu, L.; Lu, X.Y.; Xu, F.; Liu, C.F.; Shen, W.F.; Jia, N.Y.; Cheng, H.Y.; Yang, Y.F.; Shen, F. Small Intrahepatic Cholangiocarcinoma and Hepatocellular Carcinoma in Cirrhotic Livers May Share Similar Enhancement Patterns at Multiphase Dynamic MR Imaging. *Radiology* **2016**, *281*, 150–157. [CrossRef]

- 31. Galassi, M.; Iavarone, M.; Rossi, S.; Bota, S.; Vavassori, S.; Rosa, L.; Leoni, S.; Venerandi, L.; Marinelli, S.; Sangiovanni, A.; et al. Patterns of appearance and risk of misdiagnosis of intrahepatic cholangiocarcinoma in cirrhosis at contrast enhanced ultrasound. *Liver Int.* 2013, 33, 771–779. [CrossRef] [PubMed]
- 32. Iavarone, M.; Piscaglia, F.; Vavassori, S.; Galassi, M.; Sangiovanni, A.; Venerandi, L.; Forzenigo, L.V.; Golfieri, R.; Bolondi, L.; Colombo, M. Contrast enhanced CT-scan to diagnose intrahepatic cholangiocarcinoma in patients with cirrhosis. *J. Hepatol.* **2013**, 58, 1188–1193. [CrossRef] [PubMed]
- 33. Kim, S.J.; Lee, J.M.; Han, J.K.; Kim, K.H.; Lee, J.Y.; Choi, B.I. Peripheral mass-forming cholangiocarcinoma in cirrhotic liver. *AJR Am. J. Roentgenol.* **2007**, *189*, 1428–1434. [CrossRef] [PubMed]
- 34. Hanna, R.F.; Aguirre, D.A.; Kased, N.; Emery, S.C.; Peterson, M.R.; Sirlin, C.B. Cirrhosis-associated hepatocellular nodules: Correlation of histopathologic and MR imaging features. *Radiographics* **2008**, *28*, 747–769. [CrossRef]
- 35. Choi, S.Y.; Kim, Y.K.; Min, J.H.; Kang, T.W.; Jeong, W.K.; Ahn, S.; Won, H. Added value of ancillary imaging features for differentiating scirrhous hepatocellular carcinoma from intrahepatic cholangiocarcinoma on gadoxetic acid-enhanced MR imaging. *Eur. Radiol.* 2018, 28, 2549–2560. [CrossRef]
- 36. Chong, Y.S.; Kim, Y.K.; Lee, M.W.; Kim, S.H.; Lee, W.J.; Rhim, H.C.; Lee, S.J. Differentiating mass-forming intrahepatic cholangiocarcinoma from atypical hepatocellular carcinoma using gadoxetic acid-enhanced MRI. *Clin. Radiol.* **2012**, *67*, 766–773. [CrossRef]
- Potretzke, T.A.; Tan, B.R.; Doyle, M.B.; Brunt, E.M.; Heiken, J.P.; Fowler, K.J. Imaging Features of Biphenotypic Primary Liver Carcinoma (Hepatocholangiocarcinoma) and the Potential to Mimic Hepatocellular Carcinoma: LI-RADS Analysis of CT and MRI Features in 61 Cases. AJR Am. J. Roentgenol. 2016, 207, 25–31. [CrossRef]
- 38. Losic, B.; Craig, A.J.; Villacorta-Martin, C.; Martins-Filho, S.N.; Akers, N.; Chen, X.; Ahsen, M.E.; von Felden, J.; Labgaa, I.; D'Avola, D.; et al. Intratumoral heterogeneity and clonal evolution in liver cancer. *Nat. Commun.* **2020**, *11*, 291. [CrossRef]
- 39. Lambin, P.; Rios-Velazquez, E.; Leijenaar, R.; Carvalho, S.; van Stiphout, R.G.; Granton, P.; Zegers, C.M.; Gillies, R.; Boellard, R.; Dekker, A.; et al. Radiomics: Extracting more information from medical images using advanced feature analysis. *Eur. J. Cancer* **2012**, *48*, 441–446. [CrossRef]
- 40. Tao, Y.Y.; Shi, Y.; Gong, X.Q.; Li, L.; Li, Z.M.; Yang, L.; Zhang, X.M. Radiomic Analysis Based on Magnetic Resonance Imaging for Predicting PD-L2 Expression in Hepatocellular Carcinoma. *Cancers* **2023**, *15*, 365. [CrossRef]
- 41. Mao, Q.; Zhou, M.T.; Zhao, Z.P.; Liu, N.; Yang, L.; Zhang, X.M. Role of radiomics in the diagnosis and treatment of gastrointestinal cancer. *World J. Gastroenterol.* **2022**, *28*, 6002–6016. [CrossRef] [PubMed]
- 42. Huang, F.; Liu, X.; Liu, P.; Xu, D.; Li, Z.; Lin, H.; Xie, A. The Application Value of MRI T2*WI Radiomics Nomogram in Discriminating Hepatocellular Carcinoma from Intrahepatic Cholangiocarcinoma. *Comput. Math. Methods Med.* **2022**, 2022, 7099476. [CrossRef] [PubMed]
- 43. Zhou, Y.; Zhou, G.; Zhang, J.; Xu, C.; Zhu, F.; Xu, P. DCE-MRI based radiomics nomogram for preoperatively differentiating combined hepatocellular-cholangiocarcinoma from mass-forming intrahepatic cholangiocarcinoma. *Eur. Radiol.* 2022, 32, 5004–5015. [CrossRef] [PubMed]
- 44. Liu, X.; Khalvati, F.; Namdar, K.; Fischer, S.; Lewis, S.; Taouli, B.; Haider, M.A.; Jhaveri, K.S. Can machine learning radiomics provide pre-operative differentiation of combined hepatocellular cholangiocarcinoma from hepatocellular carcinoma and cholangiocarcinoma to inform optimal treatment planning? *Eur. Radiol.* 2021, 31, 244–255. [CrossRef] [PubMed]
- 45. Wang, W.; Gu, D.; Wei, J.; Ding, Y.; Yang, L.; Zhu, K.; Luo, R.; Rao, S.X.; Tian, J.; Zeng, M. A radiomics-based biomarker for cytokeratin 19 status of hepatocellular carcinoma with gadoxetic acid-enhanced MRI. *Eur. Radiol.* **2020**, *30*, 3004–3014. [CrossRef] [PubMed]
- 46. Mokrane, F.Z.; Lu, L.; Vavasseur, A.; Otal, P.; Peron, J.M.; Luk, L.; Yang, H.; Ammari, S.; Saenger, Y.; Rousseau, H.; et al. Radiomics machine-learning signature for diagnosis of hepatocellular carcinoma in cirrhotic patients with indeterminate liver nodules. *Eur. Radiol.* 2020, 30, 558–570. [CrossRef] [PubMed]
- 47. Jeong, W.K.; Jamshidi, N.; Felker, E.R.; Raman, S.S.; Lu, D.S. Radiomics and radiogenomics of primary liver cancers. *Clin. Mol. Hepatol.* **2019**, 25, 21–29. [CrossRef] [PubMed]
- 48. Jiang, H.; Liu, X.; Chen, J.; Wei, Y.; Lee, J.M.; Cao, L.; Wu, Y.; Duan, T.; Li, X.; Ma, L.; et al. Man or machine? Prospective comparison of the version 2018 EASL, LI-RADS criteria and a radiomics model to diagnose hepatocellular carcinoma. *Cancer Imaging* 2019, 19, 84. [CrossRef]
- 49. Hectors, S.J.; Lewis, S.; Besa, C.; King, M.J.; Said, D.; Putra, J.; Ward, S.; Higashi, T.; Thung, S.; Yao, S.; et al. MRI radiomics features predict immuno-oncological characteristics of hepatocellular carcinoma. *Eur. Radiol.* **2020**, *30*, 3759–3769. [CrossRef]
- 50. Chen, S.; Feng, S.; Wei, J.; Liu, F.; Li, B.; Li, X.; Hou, Y.; Gu, D.; Tang, M.; Xiao, H.; et al. Pretreatment prediction of immunoscore in hepatocellular cancer: A radiomics-based clinical model based on Gd-EOB-DTPA-enhanced MRI imaging. *Eur. Radiol.* **2019**, 29, 4177–4187. [CrossRef]
- 51. Yang, L.; Gu, D.; Wei, J.; Yang, C.; Rao, S.; Wang, W.; Chen, C.; Ding, Y.; Tian, J.; Zeng, M. A Radiomics Nomogram for Preoperative Prediction of Microvascular Invasion in Hepatocellular Carcinoma. *Liver Cancer* **2019**, *8*, 373–386. [CrossRef] [PubMed]

Cancers 2023, 15, 5373 16 of 17

52. Nebbia, G.; Zhang, Q.; Arefan, D.; Zhao, X.; Wu, S. Pre-operative Microvascular Invasion Prediction Using Multi-parametric Liver MRI Radiomics. *J. Digit. Imaging* **2020**, 33, 1376–1386. [CrossRef] [PubMed]

- 53. Ji, G.W.; Zhu, F.P.; Xu, Q.; Wang, K.; Wu, M.Y.; Tang, W.W.; Li, X.C.; Wang, X.H. Machine-learning analysis of contrast-enhanced CT radiomics predicts recurrence of hepatocellular carcinoma after resection: A multi-institutional study. *EBioMedicine* **2019**, *50*, 156–165. [CrossRef] [PubMed]
- 54. Wang, X.H.; Long, L.H.; Cui, Y.; Jia, A.Y.; Zhu, X.G.; Wang, H.Z.; Wang, Z.; Zhan, C.M.; Wang, Z.H.; Wang, W.H. MRI-based radiomics model for preoperative prediction of 5-year survival in patients with hepatocellular carcinoma. *Br. J. Cancer* 2020, 122, 978–985. [CrossRef] [PubMed]
- 55. Lubner, M.G.; Smith, A.D.; Sandrasegaran, K.; Sahani, D.V.; Pickhardt, P.J. CT Texture Analysis: Definitions, Applications, Biologic Correlates, and Challenges. *Radiographics* **2017**, *37*, 1483–1503. [CrossRef] [PubMed]
- 56. Lambin, P.; Leijenaar, R.T.H.; Deist, T.M.; Peerlings, J.; Jong, E.E.C.; Timmeren, J.T.; Sanduleanu, S.; Larue, R.T.H.L.; Even, A.J.G.; Jochems, A.; et al. Radiomics: The bridge between medical imaging and personalized medicine. *Nat. Rev. Clin. Oncol.* **2017**, *14*, 749–762. [CrossRef]
- 57. Galle, P.R.; Forner, A.; Llovet, J.M.; Mazzaferro, V.; Piscaglia, F.; Raoul, J.L.; Schirmacher, P.; Vilgrain, V. EASL Clinical Practice Guidelines: Management of hepatocellular carcinoma. *J. Hepatol.* **2018**, *69*, 182–236. [CrossRef]
- 58. Surveillance group; Diagnosis group; Staging group; Surgery group; Local ablation group; TACE/TARE/HAI group; Target therapy/systemic therapy group; Radiotherapy group; Prevention group; Drafting group. Management consensus guideline for hepatocellular carcinoma: 2016 updated by the Taiwan Liver Cancer Association and the Gastroenterological Society of Taiwan. *J. Formos. Med. Assoc.* 2018, 117, 381–403. [CrossRef]
- 59. Lee, Y.J.; Lee, J.M.; Lee, J.S.; Lee, H.Y.; Park, B.H.; Kim, Y.H.; Han, J.K.; Choi, B.I. Hepatocellular carcinoma: Diagnostic performance of multidetector CT and MR imaging-a systematic review and meta-analysis. *Radiology* **2015**, 275, 97–109. [CrossRef]
- 60. Liu, X.; Jiang, H.; Chen, J.; Zhou, Y.; Huang, Z.; Song, B. Gadoxetic acid disodium-enhanced magnetic resonance imaging outperformed multidetector computed tomography in diagnosing small hepatocellular carcinoma: A meta-analysis. *Liver Transpl.* **2017**, 23, 1505–1518. [CrossRef]
- 61. Choi, S.H.; Lee, S.S.; Kim, S.Y.; Park, H.P.; Park, S.H.; Kim, K.M.; Hong, S.M.; Yu, E.; Lee, M.G. Intrahepatic Cholangiocarcinoma in Patients with Cirrhosis: Differentiation from Hepatocellular Carcinoma by Using Gadoxetic Acid-enhanced MR Imaging and Dynamic CT. *Radiology* **2017**, 282, 771–781. [CrossRef] [PubMed]
- 62. Wei, Y.; Gao, F.; Zheng, D.; Huang, Z.; Wang, M.; Hu, F.; Chen, C.; Duan, T.; Chen, J.; Cao, L.; et al. Intrahepatic cholangiocarcinoma in the setting of HBV-related cirrhosis: Differentiation with hepatocellular carcinoma by using Intravoxel incoherent motion diffusion-weighted MR imaging. *Oncotarget* 2018, *9*, 7975–7983. [CrossRef] [PubMed]
- 63. Lewis, S.; Peti, S.; Hectors, S.J.; King, M.; Rosen, A.; Kamath, A.; Putra, J.; Thung, S.; Taouli, B. Volumetric quantitative histogram analysis using diffusion-weighted magnetic resonance imaging to differentiate HCC from other primary liver cancers. *Abdom. Radiol.* **2019**, 44, 912–922. [CrossRef] [PubMed]
- 64. Wei, M.; Lü, L.; Lin, P.; Chen, Z.; Quan, Z.; Tang, Z. Multiple cellular origins and molecular evolution of intrahepatic cholangio-carcinoma. *Cancer Lett.* **2016**, *379*, 253–261. [CrossRef]
- 65. Peng, J.; Zheng, J.; Yang, C.; Wang, R.; Zhou, Y.; Tao, Y.Y.; Gong, X.Q.; Wang, W.C.; Zhang, X.M.; Yang, L. Intravoxel incoherent motion diffusion-weighted imaging to differentiate hepatocellular carcinoma from intrahepatic cholangiocarcinoma. *Sci. Rep.* **2020**, *10*, 7717. [CrossRef]
- 66. Choi, I.Y.; Lee, S.S.; Sung, Y.S.; Cheong, H.; Lee, H.; Byun, J.B.; Kim, S.Y.; Lee, S.J.; Shin, Y.M.; Lee, M.G. Intravoxel incoherent motion diffusion-weighted imaging for characterizing focal hepatic lesions: Correlation with lesion enhancement. J. Magn. Reson. Imaging 2017, 45, 1589–1598. [CrossRef]
- 67. Shao, S.; Shan, Q.; Zheng, N.; Wang, B.; Wang, J. Role of Intravoxel Incoherent Motion in Discriminating Hepatitis B Virus-Related Intrahepatic Mass-Forming Cholangiocarcinoma from Hepatocellular Carcinoma Based on Liver Imaging Reporting and Data System v2018. *Cancer Biother. Radiopharm.* 2019, 34, 511–518. [CrossRef]
- 68. Çelebi, F.; Yaghouti, K.; Cindil, E.; Dogusoy, G.B.; Tokat, Y.; Balcı, C. The Role of 18F-FDG PET/MRI in the Assessment of Primary Intrahepatic Neoplasms. *Acad. Radiol.* **2021**, *28*, 189–198. [CrossRef]
- 69. Wang, X.; Wang, S.; Yin, X.; Zheng, Y. MRI-based radiomics distinguish different pathological types of hepatocellular carcinoma. *Comput. Biol. Med.* **2022**, *141*, 105058. [CrossRef]
- 70. Han, X.; Sun, M.; Wang, M.; Fan, R.; Chen, D.; Xie, L.; Liu, A. The enhanced T2 star weighted angiography (ESWAN) value for differentiating borderline from malignant epithelial ovarian tumors. *Eur. J. Radiol.* **2019**, *118*, 187–193. [CrossRef]
- 71. Gong, X.Q.; Tao, Y.Y.; Wu, Y.K.; Liu, N.; Yu, X.; Wang, R.; Zheng, J.; Liu, N.; Huang, X.H.; Li, J.D.; et al. Progress of MRI Radiomics in Hepatocellular Carcinoma. *Front. Oncol.* **2021**, *11*, 698373. [CrossRef] [PubMed]
- 72. Greiner, M.; Pfeiffer, D.; Smith, R.D. Principles and practical application of the receiver-operating characteristic analysis for diagnostic tests. *Prev. Vet. Med.* **2000**, *45*, 23–41. [CrossRef] [PubMed]
- 73. Zeng, D.; Zhou, R.; Yu, Y.; Luo, Y.; Zhang, J.; Sun, H.; Bin, J.; Liao, Y.; Rao, J.; Zhang, Y.; et al. Gene expression profiles for a prognostic immunoscore in gastric cancer. *Br. J. Surg.* 2018, 105, 1338–1348. [CrossRef]
- 74. Fahmy, D.; Alksas, A.; Elnakib, A.; Mahmoud, A.; Kandil, H.; Khalil, A.; Ghazal, M.; Bogaert, E.; Contractor, S.; El-Baz, A. The Role of Radiomics and AI Technologies in the Segmentation, Detection, and Management of Hepatocellular Carcinoma. *Cancers* **2022**, *14*, 6123. [CrossRef]

Cancers 2023, 15, 5373 17 of 17

75. Jiang, C.; Zhao, L.; Xin, B.; Ma, G.; Wang, X.; Song, S. 18F-FDG PET/CT radiomic analysis for classifying and predicting microvascular invasion in hepatocellular carcinoma and intrahepatic cholangiocarcinoma. *Quant. Imaging Med. Surg.* 2022, 12, 4135–4150. [CrossRef]

- 76. Xu, X.; Mao, Y.; Tang, Y.; Liu, Y.; Xue, C.; Yue, Q.; Liu, Q.; Wang, J.; Yin, Y. Classification of Hepatocellular Carcinoma and Intrahepatic Cholangiocarcinoma Based on Radiomic Analysis. *Comput. Math. Methods Med.* **2022**, 2022, 5334095. [CrossRef]
- 77. Ren, S.; Li, Q.; Liu, S.; Qi, Q.; Duan, S.; Mao, B.; Li, X.; Wu, Y.; Zhang, L. Clinical Value of Machine Learning-Based Ultrasomics in Preoperative Differentiation Between Hepatocellular Carcinoma and Intrahepatic Cholangiocarcinoma: A Multicenter Study. *Front. Oncol.* 2021, 11, 749137. [CrossRef]
- 78. Peng, Y.; Lin, P.; Wu, L.; Wan, D.; Zhao, Y.; Liang, L.; Ma, X.; Qin, H.; Liu, Y.; Li, X.; et al. Ultrasound-Based Radiomics Analysis for Preoperatively Predicting Different Histopathological Subtypes of Primary Liver Cancer. *Front. Oncol.* **2020**, *10*, 1646. [CrossRef]
- 79. Zhang, J.; Huang, Z.; Cao, L.; Zhang, Z.; Wei, Y.; Zhang, X.; Song, B. Differentiation combined hepatocellular and cholangiocarcinoma from intrahepatic cholangiocarcinoma based on radiomics machine learning. *Ann. Transl. Med.* **2020**, *8*, 119. [CrossRef]
- 80. Gao, R.; Zhao, S.; Aishanjiang, K.; Cai, H.; Wei, T.; Zhang, Y.; Liu, Z.; Zhou, J.; Han, B.; Wang, J.; et al. Deep learning for differential diagnosis of malignant hepatic tumors based on multi-phase contrast-enhanced CT and clinical data. *J. Hematol. Oncol.* 2021, 14, 154. [CrossRef]
- 81. Just, N. Improving tumour heterogeneity MRI assessment with histograms. *Br. J. Cancer* **2014**, 111, 2205–2213. [CrossRef] [PubMed]
- 82. Zhao, Y.J.; Chen, W.X.; Wu, D.S.; Zhang, W.Y.; Zheng, L.R. Differentiation of mass-forming intrahepatic cholangiocarcinoma from poorly differentiated hepatocellular carcinoma: Based on the multivariate analysis of contrast-enhanced computed tomography findings. *Abdom. Radiol.* **2016**, *41*, 978–989. [CrossRef] [PubMed]

Disclaimer/Publisher's Note: The statements, opinions and data contained in all publications are solely those of the individual author(s) and contributor(s) and not of MDPI and/or the editor(s). MDPI and/or the editor(s) disclaim responsibility for any injury to people or property resulting from any ideas, methods, instructions or products referred to in the content.